

UTILITY-DIVERSITY AWARE ONLINE BATCH SELECTION FOR LLM SUPERVISED FINE-TUNING

Heming Zou¹ Yixiu Mao¹ Yun Qu¹ Qi Wang^{1†} Xiangyang Ji^{1†}

¹Department of Automation, Tsinghua University

{zouhm24, myx21, qy22, cheemswang}@mails.tsinghua.edu.cn
xyji@tsinghua.edu.cn

ABSTRACT

Supervised fine-tuning (SFT) is a commonly used technique to adapt large language models (LLMs) to downstream tasks. In practice, SFT on a full dataset is computationally expensive and sometimes suffers from overfitting or bias amplification. This facilitates the rise of data curation in SFT, which prioritizes the most valuable data to optimize. This work studies the online batch selection family that dynamically scores and filters samples during the training process. However, existing popular methods often (i) rely merely on the utility of data to select a subset while neglecting other crucial factors like diversity, (ii) rely on external resources such as reference models or validation sets, and (iii) incur extra training time over full-dataset training. To address these limitations, this work develops **UDS (Utility-Diversity Sampling)**, a framework for efficient online batch selection in SFT. UDS leverages the nuclear norm of the logits matrix to capture both data utility and intra-sample diversity, while estimating inter-sample diversity through efficient low-dimensional embedding comparisons with a lightweight memory buffer of historical samples. Such a design eliminates the need for external resources and unnecessary backpropagation, securing computational efficiency. Experiments on multiple benchmarks demonstrate that UDS consistently outperforms state-of-the-art online batch selection methods under varying data budgets, and significantly reduces training time compared to full-dataset fine-tuning. Code is available at <https://github.com/gfyddha/UDS>.

1 INTRODUCTION

The rapid progress of Large Language Models (LLMs) has reshaped natural language processing and enabled impressive generalization across a wide range of domains (Achiam et al., 2023; Brown et al., 2020; Liu et al., 2024; Touvron et al., 2023; Bai et al., 2023). To further improve their performance in specialized areas, Supervised Fine-tuning (SFT) has emerged as a typical post-training paradigm. However, training on a full dataset is not always advantageous. It entails substantial computational cost and has been shown to be less effective than using a small amount of carefully curated data (Albalak et al., 2024; Xia et al., 2024; Zhou et al., 2023). These challenges highlight the importance of principled data selection strategies that can improve both efficiency and effectiveness in SFT.

In this work, we address this challenge by focusing on **online batch selection**, a paradigm that dynamically evaluates sample value and performs filtering during training (Wang et al., 2024; Loshchilov & Hutter, 2015; Katharopoulos & Fleuret, 2018; Mindermann et al., 2022). Instead of using all samples in a batch, the model assesses the importance of each sample as it is encountered and selects only a subset to participate in parameter updates. This approach enables the selection process to adapt in real time to the model’s current state and learning trajectory, improving both training efficiency and effectiveness.

However, despite promising progress, current online batch selection methods still face several issues that hinder their practical deployment. These methods typically rely solely on *data utility*, e.g., picking sample subsets with high loss (Loshchilov & Hutter, 2015; Jiang et al., 2019) or gradient magnitude (Katharopoulos & Fleuret, 2018). While such heuristics enable capturing the critical

[†]Corresponding author

Table 1: **Comparison of online batch selection methods under our desiderata (D1–D3).** The columns denote: Data Utility, Intra-sample Div. (Intra-sample Diversity), Inter-sample Div. (Inter-sample Diversity), No External Res. (No External Resources), and Train. Time Reduc. (Training Time Reduction). The symbols denote: ✓ (support), and ✗ (don’t support).

Method	Data Utility	Intra-sample Div.	Inter-sample Div.	No External Res.	Train. Time Reduc.
Max Loss	✓	✗	✗	✓	✓
Max Grad	✓	✗	✗	✓	✗
RHO-Loss	✓	✗	✗	✗	✗
GREATS	✓	✗	✓	✗	✗
UDS (Ours)	✓	✓	✓	✓	✓

samples to reduce the current training loss, they evaluate sample value from a limited perspective. In practice, effective selection also requires considerations of *intra-sample diversity*, to reflect the richness of information with fewer repetitive phrases within each training instance, and *inter-sample diversity* to suppress redundancy across examples by avoiding repeated training on near-duplicate content (Lee et al., 2021; Tirumala et al., 2023). Popular literature (Loshchilov & Hutter, 2015; Katharopoulos & Fleuret, 2018; Mindermann et al., 2022) prioritizes data utility and rarely examines the selection criteria through the lens of diversity.

Another primary issue involves both *external dependencies* and *computational overhead*. Some approaches (Mindermann et al., 2022; Wang et al., 2024) rely on a held-out validation set, which may be unavailable since we hardly know the exact distribution of test dataset. Other methods (Mindermann et al., 2022; Deng et al., 2023) use a reference model that is also shown to be impractical in the real world (Kaddour et al., 2023). Besides these external dependencies, several selection algorithms (Katharopoulos & Fleuret, 2018; Wang et al., 2024; Mindermann et al., 2022) introduce substantial computational costs that even exceed the expense of full-dataset training, raising efficiency concerns.

Based on the above evidence, this work proposes that an ideal online batch selection method should be comprehensive and satisfy the three desiderata (D1–D3) outlined below. A systematic comparison of representative methods against these criteria is summarized in Table 1.

D1: Jointly consider *data utility*, *intra-sample diversity*, and *inter-sample diversity*;

D2: Circumvent the access to external resources, e.g., reference model or validation set;

D3: Reduce the training time of the overall pipeline relative to the full-dataset SFT.

Leveraging logits as basis for online scoring. To operationalize these desiderata, a key challenge lies in how to efficiently and reliably score candidate samples during training. In online batch selection, each candidate sample must be evaluated under the current model to quantify its contribution to learning. This evaluation typically requires at least a forward pass, as it can fully capture how the model presently interprets the sample and thus provide an accurate basis for selection (Huang et al., 2023; Shorinwa et al., 2025). To achieve this efficiently (D3) without external resources (D2), we must avoid expensive gradient computations for each candidate sample and leverage intrinsic signals already available during forward propagation. These considerations collectively justify leveraging the model’s output logits, which are naturally produced during the forward pass and encode rich information about both sample utility and diversity (Qiu & Miikkulainen, 2024; Geng et al., 2023). Specifically, we compute an *intra-sample importance score* based on the nuclear norm of the logits, which captures the utility and intra-sample diversity of a sample, and an *inter-sample importance score* using low-dimensional similarity matching against previously selected samples to quantify inter-sample diversity (D1). Integrating these scores allows the training process to balance exploitation of high-utility samples with exploration of less-visited regions in the data distribution, thereby improving the overall effectiveness of online batch selection.

In summary, we present **UDS (Utility-Diversity Sampling)**, a new framework for online batch selection in SFT of LLMs. Our main contributions are:

1. To capture intra-sample value, we leverage the nuclear norm of the logits matrix, which naturally reflects both *data utility* and *intra-sample diversity*, providing a principled criterion for assessing within-sample informativeness.

2. To estimate inter-sample diversity, we design a structured bilinear random projection of logits for compact embedding and show that similarity matching with historical data points effectively reduces redundancy with negligible overhead.
3. Our UDS operates directly on forward-pass outputs without external resources, achieving faster convergence than full-dataset SFT and surpassing existing online batch selection baselines.

2 PRELIMINARIES

2.1 PROBLEM FORMULATION OF ONLINE BATCH SELECTION

At training iteration t , we draw a candidate batch $\mathcal{B}_t = \{(\mathbf{x}_t^i, y_t^i)\}_{i=1}^B$ from the corpus. The goal of online batch selection is to choose a subset $\widehat{\mathcal{B}}_t \subseteq \mathcal{B}_t$ that maximizes the immediate (or near-term) benefit to the model. Let $s(\mathbf{x}_t^i; \boldsymbol{\theta}_t, \mathcal{H}_t) \in \mathbb{R}$ denote a per-sample importance score computed under the current model state $\boldsymbol{\theta}_t$ and optional history \mathcal{H}_t (e.g., a small buffer of recent embeddings). The selection objective can be viewed as an optimization problem:

$$\widehat{\mathcal{B}}_t = \arg \max_{S \subseteq \mathcal{B}_t, |S|=K} \sum_{i \in S} s(\mathbf{x}_t^i; \boldsymbol{\theta}_t, \mathcal{H}_t), \quad (1)$$

where K controls the fraction of data we aim to select.

2.2 AUTOREGRESSIVE LANGUAGE MODELING

Our work focuses on autoregressive language models that factorize the sequence probability via the chain rule:

$$p_{\boldsymbol{\theta}_t}(\mathbf{x}_t^i) = \prod_{n=1}^N p_{\boldsymbol{\theta}_t}(x_t^{i,n} | \mathbf{x}_t^{i,< n}), \quad (2)$$

where $\mathbf{x}_t^{i,< n} = (x_t^{i,1}, \dots, x_t^{i,n-1})$ denotes the context prefix, and $\boldsymbol{\theta}_t \in \mathbb{R}^p$ represents model parameters at iteration t . At each generation step n , model $\pi_{\boldsymbol{\theta}_t}$ produces a logit vector $\mathbf{l}_t^{i,n} \in \mathbb{R}^V$ over vocabulary \mathcal{V} , with $V = |\mathcal{V}|$ the vocabulary size. For a sequence of length N , these vectors $\mathbf{l}_t^{i,1}, \dots, \mathbf{l}_t^{i,N}$ collectively form the logits matrix $\mathbf{L}(\mathbf{x}_t^i; \boldsymbol{\theta}_t) \in \mathbb{R}^{N \times V}$, where the n -th row corresponds to logits at position n . $\mathbf{L}(\mathbf{x}_t^i; \boldsymbol{\theta}_t)$ captures the model’s predictive distribution at each position. Applying the softmax function to each row of $\mathbf{L}(\mathbf{x}_t^i; \boldsymbol{\theta}_t)$ yields the conditional probability distribution for the next token. The resulting probability matrix is denoted $\mathbf{P}(\mathbf{x}_t^i; \boldsymbol{\theta}_t) \in \mathbb{R}^{N \times V}$, with entries

$$p_{\boldsymbol{\theta}_t}(x_t^{i,n} | \mathbf{x}_t^{i,< n}) = \frac{\exp(\pi_{\boldsymbol{\theta}_t}(\mathbf{x}_{< n})[x_n])}{\sum_{y \in \mathcal{V}} \exp(\pi_{\boldsymbol{\theta}_t}(\mathbf{x}_{< n})[y])}. \quad (3)$$

During fine-tuning, the parameters $\boldsymbol{\theta}_t$ are updated to maximize the likelihood of training sequences. At iteration t , the online selection mechanism identifies an informative subset $\widehat{\mathcal{B}}_t$ from the candidate batch \mathcal{B}_t , which is then used to perform a gradient update $\boldsymbol{\theta}_t \rightarrow \boldsymbol{\theta}_{t+1}$.

3 UTILITY-DIVERSITY SAMPLING (UDS)

We propose **UDS**, an online batch selection framework that jointly considers data utility, intra-sample diversity, and inter-sample diversity. It scores and samples each data point using a mixture of two complementary scores: (i) the *Nuclear Norm* of the logits matrix ($s_{\text{intra}}^{t,i}$), capturing optimization utility and intra-sample diversity; and (ii) the *Diversity Distance* ($s_{\text{inter}}^{t,i}$), measuring dispersion against recent selections. An overview is shown in Figure 1, with pseudocode provided in Algorithm 1.

3.1 INTRA-SAMPLE IMPORTANCE SCORE VIA NUCLEAR NORM

The intra-sample importance score ($s_{\text{intra}}^{t,i}$) can be characterized through two complementary views: (i) *optimization utility*—how much the sample can contribute to loss reduction during training, and (ii) *intra-sample diversity*—how diverse the model’s token-level outputs are within the sequence. We

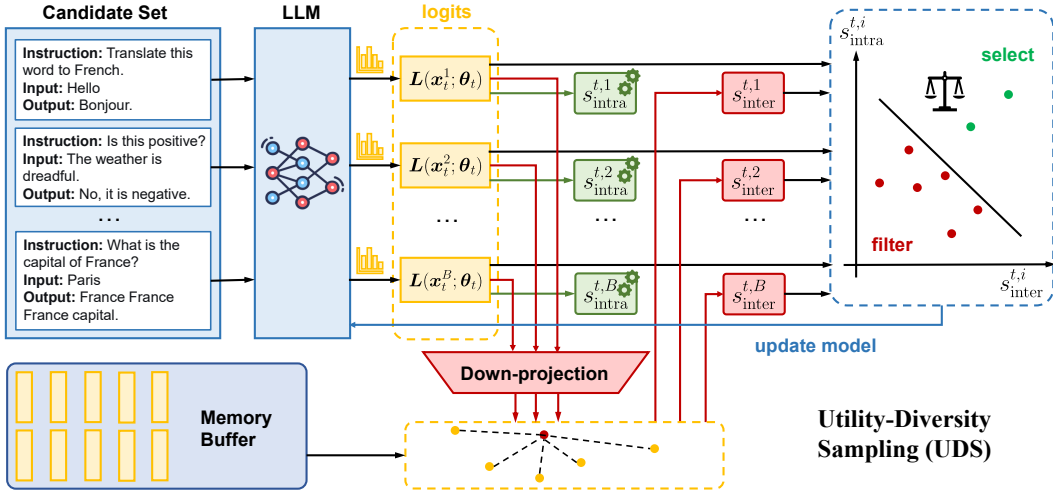


Figure 1: **Schematic of the UDS Framework.** In the forward pass, the LLM extract logits $\mathbf{L}(\mathbf{x}_t^i; \theta_t)$ for each sample. Using $\mathbf{L}(\mathbf{x}_t^i; \theta_t)$, we first calculate its nuclear norm for the intra-sample importance score $s_{\text{intra}}^{t,i}$, and then down-projected to calculate the distance $s_{\text{inter}}^{t,i}$ with historical samples in the memory buffer. Finally, we select the top- K valuable samples to update the LLM.

employ the nuclear norm (trace norm) of the logits matrix $\mathbf{L}(\mathbf{x}_t^i; \theta_t)$ to capture both aspects. The nuclear norm $\|\mathbf{L}(\mathbf{x}_t^i; \theta_t)\|_*$ is defined as the sum of singular values of $\mathbf{L}(\mathbf{x}_t^i; \theta_t)$. Let $\{\sigma_1, \sigma_2, \dots, \sigma_r\}$ denote its singular values (with $r = \text{rank}(\mathbf{L}(\mathbf{x}_t^i; \theta_t))$), then $s_{\text{intra}}^{t,i}$ is computed as:

$$s_{\text{intra}}^{t,i} = \|\mathbf{L}(\mathbf{x}_t^i; \theta_t)\|_* = \sum_{j=1}^r \sigma_j. \quad (4)$$

In mathematics, the nuclear norm and the Frobenius norm can bound each other, as shown in Lemma 3.1. A detailed explanation is provided in Appendix C.1.

Lemma 3.1. (Horn & Johnson, 2012) For any matrix $\mathbf{L}(\mathbf{x}_t^i; \theta_t) \in \mathbb{R}^{N \times V}$, the following inequality holds:

$$\|\mathbf{L}(\mathbf{x}_t^i; \theta_t)\|_F \leq \|\mathbf{L}(\mathbf{x}_t^i; \theta_t)\|_* \leq \sqrt{\min(N, V)} \|\mathbf{L}(\mathbf{x}_t^i; \theta_t)\|_F,$$

where $\|\cdot\|_F$ denotes the Frobenius norm, computed as the square root of the sum of squares of all entries in the matrix. The left inequality achieves equality when $\mathbf{L}(\mathbf{x}_t^i; \theta_t)$ is rank-1 and has only one non-zero singular value. The right inequality achieves equality when $\mathbf{L}(\mathbf{x}_t^i; \theta_t)$ has full rank and all singular values are equal.

Thus, a larger nuclear norm arises in two ways: (1) the Frobenius norm increases, indicating larger logits, and (2) for a fixed Frobenius norm, the nuclear norm shifts closer to the upper bound. Below we clarify how these two effects embody the two complementary aspects of sample-importance score.

Larger Nuclear Norm indicates higher Optimization Utility. Traditional notions of sample difficulty—such as *maximum loss* (Loshchilov & Hutter, 2015) or *maximum gradient* (Katharopoulos & Fleuret, 2018)—often misalign with actual training dynamics (Wang et al., 2024). Instead, we characterize sample importance through its potential contribution to loss reduction, termed its *optimization utility*. For ease of exposition, we assume training with SGD using batch size B and a learning rate η_t . An extension to Adam is provided in Appendix C.2. The parameter update at iteration t is $\theta_{t+1} - \theta_t = -\frac{\eta_t}{B} \sum_{j=1}^B \nabla_{\theta} \ell(\mathbf{x}_t^j; \theta_t)$. After the update, the logits matrix for datapoint

Algorithm 1 Utility-Diversity Sampling (UDS)

Input: Candidate batch \mathcal{B}_t ($t = 0, 1, \dots, T$), initial model π_{θ_0} , memory queue Q

- 1: Initialize memory queue $Q \leftarrow \{\}$
- 2: **for** $t = 0, 1, \dots, T$ **do**
- 3: **// Calculate importance score and dynamically sampling**
- 4: **for** each sample $\mathbf{x}_t^i \in \mathcal{B}_t$ **do**
- 5: Perform forward pass to obtain logits $\mathbf{L}(\mathbf{x}_t^i; \theta_t) \leftarrow \pi_{\theta_t}(\mathbf{x}_t^i)$
- 6: Calculate intra-sample importance score $s_{\text{intra}}^{t,i} \leftarrow \|\mathbf{L}(\mathbf{x}_t^i; \theta_t)\|_*$
- 7: Randomly project to low-dimensional embeddings $\mathbf{z}_t^i \leftarrow \text{vec}(\mathbf{\Gamma}_2 \cdot \mathbf{L}(\mathbf{x}_t^i; \theta_t) \cdot \mathbf{\Gamma}_1^\top)$
- 8: Calculate inter-sample importance score $s_{\text{inter}}^{t,i} \leftarrow \frac{1}{|Q|} \sum_{\mathbf{z}_j \in Q} \|\mathbf{z}_t^i - \mathbf{z}_j\|_2$
- 9: Combine intra- and inter-sample importance scores $s_{\text{total}}^{t,i} = s_{\text{intra}}^{t,i} + \alpha * s_{\text{inter}}^{t,i}$
- 10: **end for**
- 11: Dynamically select top- K samples $\widehat{\mathcal{B}}_t \leftarrow \text{TopK}(\{s_{\text{total}}^{t,i}\}_{i=1}^B, K)$
- 12: **// Update memory queue**
- 13: **while** $|Q| + K > M$ **do**
- 14: $Q \leftarrow Q \setminus \{\text{oldest element}\}$
- 15: **end while**
- 16: $Q \leftarrow Q \cup \{\mathbf{z}_t^i \mid \mathbf{x}_t^i \in \widehat{\mathcal{B}}_t\}$
- 17: Update model parameters $\theta_{t+1} \leftarrow \theta_t$ through backpropagation
- 18: **end for**

\mathbf{x}_t^i can be expanded using a first-order Taylor expansion:

$$\mathbf{L}(\mathbf{x}_t^i; \theta_{t+1}) \approx \mathbf{L}(\mathbf{x}_t^i; \theta_t) + \nabla_{\theta} \mathbf{L}(\mathbf{x}_t^i; \theta_t) \cdot (\theta_{t+1} - \theta_t), \quad (5)$$

so that the induced change is

$$\delta \mathbf{L}(\mathbf{x}_t^i; \theta_t) = \mathbf{L}(\mathbf{x}_t^i; \theta_{t+1}) - \mathbf{L}(\mathbf{x}_t^i; \theta_t) \approx -\frac{\eta_t}{B} \nabla_{\theta} \mathbf{L}(\mathbf{x}_t^i; \theta_t) \cdot \left(\sum_{j=1}^B \nabla_{\theta} \ell(\mathbf{x}_t^j; \theta_t) \right). \quad (6)$$

Rather than reasoning in parameter space, we can view the training step as producing a logits perturbation $\delta \mathbf{L}(\mathbf{x}_t^i; \theta_t)$. The first-order Taylor expansion of the loss around $\mathbf{L}(\mathbf{x}_t^i; \theta_t)$ gives

$$\delta \ell(\mathbf{x}_t^i; \theta_t) := \ell(\mathbf{L}(\mathbf{x}_t^i; \theta_t) + \delta \mathbf{L}(\mathbf{x}_t^i; \theta_t)) - \ell(\mathbf{L}(\mathbf{x}_t^i; \theta_t)) \approx \langle \nabla_{\mathbf{L}} \ell(\mathbf{L}(\mathbf{x}_t^i; \theta_t)), \delta \mathbf{L}(\mathbf{x}_t^i; \theta_t) \rangle, \quad (7)$$

where $\langle \cdot, \cdot \rangle$ denotes the Frobenius inner product, and $\nabla_{\mathbf{L}} \ell(\mathbf{L}(\mathbf{x}_t^i; \theta_t))$ is the gradient matrix of ℓ with respect to \mathbf{L} . For cross-entropy loss, $\nabla_{\mathbf{L}} \ell(\mathbf{L}(\mathbf{x}_t^i; \theta_t)) = \mathbf{P}(\mathbf{x}_t^i; \theta_t) - \mathbf{Y}(\mathbf{x}_t^i)$, which we denote as $\Delta(\mathbf{x}_t^i; \theta_t)$. Hence,

$$\delta \ell(\mathbf{x}_t^i; \theta_t) \approx \langle \Delta(\mathbf{x}_t^i; \theta_t), \delta \mathbf{L}(\mathbf{x}_t^i; \theta_t) \rangle. \quad (8)$$

Intuitively, as the Frobenius norm of the logits $\|\mathbf{L}(\mathbf{x}_t^i; \theta_t)\|_F$ increases, the perturbation $\delta \mathbf{L}(\mathbf{x}_t^i; \theta_t)$ also tends to grow uniformly. This occurs because each entry in the activation logits becomes larger, and these values are directly used during backpropagation. In contrast, $\Delta(\mathbf{x}_t^i; \theta_t)$ is less sensitive to scale because it depends only on the normalized probabilities and the one-hot labels. Therefore, $\|\mathbf{L}(\mathbf{x}_t^i; \theta_t)\|_F$, $\|\mathbf{L}(\mathbf{x}_t^i; \theta_t)\|_*$, and the attainable loss reduction $-\delta \ell(\mathbf{x}_t^i; \theta_t)$ typically grow in tandem. Empirically, Figure 2 confirms a strong correlation between a sample's loss reduction and its nuclear norm. Hence, the nuclear norm can serve as an indicator of a sample's optimization utility.

When a single sample induces a larger loss reduction, it indicates that the sample both challenges the model's current predictions and provides informative gradients that effectively guide parameter updates. Such samples are particularly valuable for data selection: they not only highlight under-learned regions of the input space, but also accelerate training by yielding stronger optimization signals compared to redundant or already well-learned samples. We provide a categorization of the loss before and after training in Table 2. Hence, we prioritize selecting samples with larger nuclear norm that are more likely to have higher loss reduction.

Larger Nuclear Norm indicates higher Intra-sample Diversity. Beyond optimization utility, a larger nuclear norm can also arise from the structural diversity of token-level output distributions within a sequence. Recall Lemma 3.1: for a fixed Frobenius norm, the nuclear norm achieves its

minimum when $L(x_t^i; \theta_t)$ is rank-1 with only one singular value, and its maximum when $L(x_t^i; \theta_t)$ has full rank with equal singular values. These two extremes correspond to distinct regimes of intra-sample diversity. The lower bound typically occurs when the model predicts only a single vocabulary token throughout the sequence (indicating repetitive generation behavior), while the upper bound is achieved when the model produces a florid and diverse vocabulary distribution across tokens (reflecting richer semantic information content). Figure 3 presents a simplified example illustrating what intra-sample diversity means in real cases. Intuitively, A larger nuclear norm implies that more vocabularies in this sequence are predicted and utilized, indicating higher prediction dispersity. Specific explanations are listed below.

Low Nuclear Norm Indicates Low rank and collinear rows (low diversity). Considering the lower bound of Lemma 3.1, since $L(x_t^i; \theta_t)$ is rank-1, the row vectors l_n are nearly collinear, i.e., $l_n \approx \alpha_n v$ for some fixed v . This degenerate spectral structure indicates minimal diversity: the model’s predictions for different tokens are aligned along the same direction, resulting in repetitive output.

High Nuclear Norm Indicates High rank and orthogonal rows (high diversity). Considering the higher bound of Lemma 3.1, $L(x_t^i; \theta_t)$ has full rank and all singular values are approximately equal. This occurs when the row vectors are diverse and orthogonal with comparable norms. This flat spectrum indicates maximal diversity: each token is semantically meaningful to the output, and predictions are spread across diverse directions, capturing a wide range of semantic information.

Table 2: **Categorization of training samples by initial and final loss.** The optimization utility depends on how much the training loss decreases after training. **Green** entries denote high-utility samples that should be preferentially selected, while **Red** entries denote low-utility ones that should generally be avoided.

Before/After	High	Low
High	Too Hard	Informative
Low	Overfitted	Too Easy

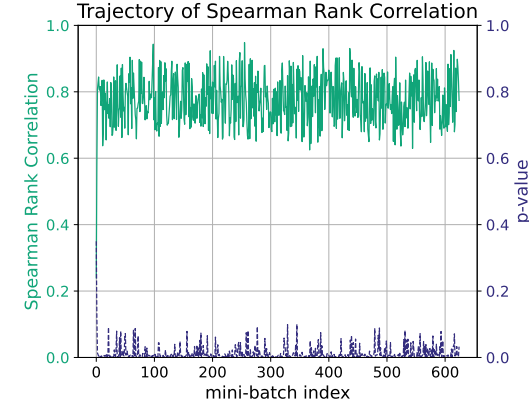


Figure 2: Strong correlation between $-\delta\ell(x_t^i; \theta_t)$ and $\|L(x_t^i; \theta_t)\|_*$ during the training process. Each point represents the correlation coefficient calculated from B pairs of values within a single batch. We extract the result using Qwen-2.5-7B on MMLU.

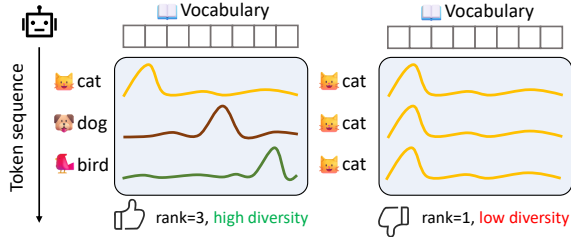


Figure 3: **Illustration of Intra-sample Diversity.** **Left:** Token sequence with high diversity, where the model predicts varied tokens (cat, dog, bird). **Right:** Token sequence with low diversity, where the model predominantly predicts a single token (cat).

3.2 INTER-SAMPLE IMPORTANCE SCORE VIA LOW-RANK SIMILARITY MATCHING

Current online batch selection methods (Wang et al., 2024) only consider sample diversity within the candidate batch, which is suboptimal because the capacity of the batch is much smaller than the global datasets. To enhance global diversity, we maintain a fixed-size First-In-First-Out (FIFO) memory buffer $Q \in \mathbb{R}^{M \times d}$, which stores representations $z \in \mathbb{R}^d$ of the last M samples selected for training ($M \gg B$), and measure inter-sample diversity by calculating the distance between the candidate sample and the recent training history.

Diversity Distance: The inter-sample diversity score for the i -th sample is computed as its average Euclidean distance to all representations in the memory buffer:

$$s_{\text{inter}}^{t,i} = \frac{1}{|Q|} \sum_{z_j \in Q} \|z_t^i - z_j\|_2. \quad (9)$$

If Q is empty, $s_{\text{inter}}^{t,i}$ is set to zero. A high $s_{\text{inter}}^{t,i}$ indicates a large distinction from recent data.

Low-dimensional Projection. As mentioned, the logits matrix $\mathbf{L}(\mathbf{x}_t^i; \boldsymbol{\theta}_t) \in \mathbb{R}^{N \times V}$ is semantically meaningful for computing diversity, but directly storing the whole matrix in the memory buffer is prohibitive (e.g., ~ 74 GB for 1024 samples in Qwen-2.5-7B). A natural strategy is to randomly project it into low-dimensional vectors $z_t^i \in \mathbb{R}^d$, while preserving pairwise distances (Johnson et al., 1984). However, a direct projection using $\boldsymbol{\Gamma} \in \mathbb{R}^{NV \times d}$ also incurs severe storage cost for the down-projection matrix (~ 74 GB in Qwen-2.5-7B if d is set to 1024). To avoid this, we try to factorize $\boldsymbol{\Gamma}$ into two smaller projections: $\boldsymbol{\Gamma}_1 \in \mathbb{R}^{d_1 \times V}$ reducing the vocabulary dimension and $\boldsymbol{\Gamma}_2 \in \mathbb{R}^{d_2 \times N}$ reducing the sequence length dimension, which together approximate the original projection with $d = d_1 d_2$. Formally, we aim to find proper $\boldsymbol{\Gamma}_1$ and $\boldsymbol{\Gamma}_2$ that operate in the following way:

$$\mathbf{z} = \text{vec}(\boldsymbol{\Gamma}_2 \cdot \mathbf{L}(\mathbf{x}_t^i; \boldsymbol{\theta}_t) \cdot \boldsymbol{\Gamma}_1^\top), \quad (10)$$

Fortunately, the *subsampled randomized Fourier transform* (SRFT)-style construction for $\boldsymbol{\Gamma}_1$ and $\boldsymbol{\Gamma}_2$ (see Theorem 3.2) can fulfill this role (Ailon & Chazelle, 2006; Jin et al., 2021). This approach achieves an approximate Johnson-Lindenstrauss embedding while avoiding the storage of an explicit $NV \times d$ projection matrix and reduces the computational complexity from $\mathcal{O}(NVd)$ to $\mathcal{O}((N + V)d \log(NV))$. The complete proof is provided in Appendix C.3.

Theorem 3.2. Let $N, V \in \mathbb{N}$, and choose $d_1 \leq V$, $d_2 \leq N$ with $d = d_1 d_2$. Define

$$\boldsymbol{\Gamma}_1 = \sqrt{\frac{V}{d_1}} \mathbf{S}_1 \mathbf{F}_1 \mathbf{D}_1 \in \mathbb{R}^{d_1 \times V}, \quad \boldsymbol{\Gamma}_2 = \sqrt{\frac{N}{d_2}} \mathbf{S}_2 \mathbf{F}_2 \mathbf{D}_2 \in \mathbb{R}^{d_2 \times N},$$

where $\mathbf{F}_1, \mathbf{F}_2$ are orthonormal transforms (discrete Fourier transform (DFT) matrices), $\mathbf{D}_1, \mathbf{D}_2$ are random $\{\pm 1\}$ diagonal matrices with independent Rademacher entries on the diagonal, and $\mathbf{S}_1, \mathbf{S}_2$ are random selection matrices that choose d_1 and d_2 rows uniformly at random without replacement. For each $\mathbf{L}(\mathbf{x}_t^i; \boldsymbol{\theta}_t) \in \mathbb{R}^{N \times V}$, define

$$\mathbf{u}_t^i = \text{vec}(\mathbf{L}(\mathbf{x}_t^i; \boldsymbol{\theta}_t)) \in \mathbb{R}^{NV}, \quad \mathbf{v}_t^i = \text{vec}(\boldsymbol{\Gamma}_2 \cdot \mathbf{L}(\mathbf{x}_t^i; \boldsymbol{\theta}_t) \cdot \boldsymbol{\Gamma}_1^\top) \in \mathbb{R}^d.$$

Then there exists a constant $C > 0$ such that for any ϵ and a finite set of n points, if $d \geq C\epsilon^{-2} \log(NV) \text{polylog}(n)$, the mapping $\mathbf{u}_t^i \mapsto \mathbf{v}_t^i$ satisfies the Johnson-Lindenstrauss lemma with high probability. Then, for all i, j ,

$$(1 - \epsilon) \|\mathbf{u}_t^i - \mathbf{u}_t^j\|_2^2 \leq \|\mathbf{v}_t^i - \mathbf{v}_t^j\|_2^2 \leq (1 + \epsilon) \|\mathbf{u}_t^i - \mathbf{u}_t^j\|_2^2.$$

3.3 SELECTION CRITERION

After computing the intra- and inter-sample importance scores $s_{\text{intra}}^{t,i}$ and $s_{\text{inter}}^{t,i}$, we combine them to obtain a joint score for each sample:

$$s_{\text{total}}^{t,i} = s_{\text{intra}}^{t,i} + \alpha s_{\text{inter}}^{t,i}, \quad (11)$$

where α is a trade-off factor. Based on $s_{\text{total}}^{t,i}$, we then select the top- K samples from the current batch \mathcal{B}_t for training:

$$\widehat{\mathcal{B}}_t = \arg \max_{S \subseteq \mathcal{B}_t, |S|=K} \sum_{i \in S} s_{\text{total}}^{t,i}. \quad (12)$$

The resulting subset selection module is plug-and-play, directly integrating with the SFT pipeline to enhance its performance while maintaining efficiency.

Table 3: **Performance Comparison for Different Online Batch Selection Methods.** We evaluate various methods across four benchmarks: MMLU, ScienceQA, GSM8K, and HumanEval. \bar{A} denotes average accuracy or Pass@1 reported in percentage (%). $\mathcal{T}_{\text{train}}$ denotes throughput during the training time (samples per second). The best results of \bar{A} are highlighted in **bold**. Methods training faster than the full dataset are marked in █, others are marked in █.

Model	Method	MMLU		ScienceQA		GSM8K		HumanEval	
		$\bar{A}(\uparrow)$	$\mathcal{T}_{\text{train}}(\uparrow)$	$\bar{A}(\uparrow)$	$\mathcal{T}_{\text{train}}(\uparrow)$	$\bar{A}(\uparrow)$	$\mathcal{T}_{\text{train}}(\uparrow)$	$\bar{A}(\uparrow)$	$\mathcal{T}_{\text{train}}(\uparrow)$
Llama-3.1-8B	Regular	38.24 \pm 0.35	2.09	93.19 \pm 0.65	6.61	55.95 \pm 0.47	3.73	29.28 \pm 0.48	5.77
	Random	35.47 \pm 1.25	3.74	92.86 \pm 0.27	10.06	54.89 \pm 0.73	6.68	26.74 \pm 0.56	8.92
	MaxLoss	35.62 \pm 0.79	2.75	92.82 \pm 0.21	7.49	55.42 \pm 0.35	4.98	27.23 \pm 0.27	6.62
	MaxGrad	35.91 \pm 1.17	0.29	92.77 \pm 0.24	0.94	55.08 \pm 0.58	0.53	26.89 \pm 0.74	0.80
	RHO-Loss	37.63 \pm 0.67	1.40	93.42 \pm 0.15	3.83	56.54 \pm 0.52	2.53	27.18 \pm 0.29	3.36
	GREATS	39.04 \pm 0.29	1.88	93.68 \pm 0.19	6.04	57.03 \pm 0.33	3.37	28.56 \pm 0.34	5.25
UDS (Ours)		40.16\pm0.58	2.48	94.33\pm0.28	7.46	58.98\pm0.24	4.59	30.96\pm0.69	6.41
Qwen-2.5-7B	Regular	55.32 \pm 0.79	2.27	94.56 \pm 0.17	7.05	78.23 \pm 0.07	3.77	45.82 \pm 0.41	6.24
	Random	54.26 \pm 1.85	9.29	93.28 \pm 0.35	10.27	77.69 \pm 0.29	9.18	40.20 \pm 1.18	9.35
	MaxLoss	54.51 \pm 1.37	5.93	93.05 \pm 0.40	7.93	77.78 \pm 0.36	5.45	41.34 \pm 0.83	6.92
	MaxGrad	54.33 \pm 0.69	0.31	93.86 \pm 0.51	0.98	77.62 \pm 0.28	0.53	40.83 \pm 0.41	0.88
	RHO-Loss	57.08 \pm 0.74	1.94	93.80 \pm 0.25	3.89	78.38 \pm 0.43	3.08	43.08 \pm 1.62	3.53
	GREATS	58.19 \pm 0.49	2.12	94.17 \pm 0.62	6.53	78.61 \pm 0.41	3.50	45.04 \pm 0.59	5.80
UDS (Ours)		63.34\pm0.36	3.41	95.19\pm0.22	7.85	79.91\pm0.23	4.99	46.28\pm0.35	6.81

4 EXPERIMENTS

4.1 EXPERIMENTAL SETUP

Datasets and Backbones: We evaluate online batch selection methods’ performance across four key domains: (1) *general knowledge understanding* using the MMLU (Hendrycks et al., 2021) benchmark, with auxiliary training datasets for fine-tuning and the official test set for evaluation; (2) *scientific question answering* using ScienceQA (Lu et al., 2022) for both fine-tuning and evaluation; (3) *mathematical reasoning* on GSM8K (Cobbe et al., 2021) for both fine-tuning and evaluation; and (4) *code generation* using CodeAlpaca-20k (Chaudhary, 2023) for training and HumanEval (Chen et al., 2021) for evaluation. All experiments are conducted using Llama-3.1-8B (Grattafiori et al., 2024) and Qwen-2.5-7B (Yang et al., 2024) as backbone models following (Zou et al., 2025).

Baselines: We compare UDS against the following baselines: (1) **Regular**, where all samples are used without data selection; (2) **Random Selection**, which randomly chooses samples from batches; (3) **MaxLoss** (Loshchilov & Hutter, 2015), which prioritizes samples with the highest training loss; (4) **MaxGrad** (Katharopoulos & Fleuret, 2018), which selects samples with the largest gradient norms; (5) **RHO-Loss** (Mindermann et al., 2022), a representative method using a reference model; and (6) **GREATS** (Wang et al., 2024), a state-of-the-art (SOTA) online batch selection approach. All baselines select the same fraction of data for a fair comparison.

Implementation Details: Under hardware constraints, we employ LoRA (rank=8) for SFT training. The batch size is set to $B = 8$ for all datasets. The optimal data selection ratio is highly dependent on both the backbone model and the dataset; the ratios we adopt for different combinations of backbones and datasets are reported in Table 5. We report average accuracy on MMLU, ScienceQA, and GSM8K, and Pass@1 for HumanEval. We also compare training speed by throughput relative to an NVIDIA GeForce RTX 3090 GPU, following Wang et al. (2024). All benchmarks use zero-shot evaluation and are repeated four times with different random seeds. More detailed experimental settings are provided in Appendix D.

4.2 HIGHEST ACCURACY WITH LOWER TRAINING TIME THAN FULL DATASET

UDS achieves the highest accuracy. Across all four benchmarks, UDS consistently delivers the best accuracy among online batch selection methods. On MMLU, it achieves 63.34%, outperform-

Table 4: **Ablation study of UDS components across multiple benchmarks using Qwen-2.5-7B.** \bar{A} denotes average accuracy or Pass@1 reported in percentage (%). We report \bar{A} and relative improvement Δ over the baseline.

Method	MMLU		ScienceQA		GSM8K		HumanEval	
	\bar{A} (%)	Δ						
Random (Baseline)	54.26 \pm 1.85	–	93.28 \pm 0.35	–	77.69 \pm 0.29	–	40.20 \pm 1.18	–
Only Nuclear Norm	58.35 \pm 0.76	+4.09	94.19 \pm 0.31	+0.91	79.22 \pm 0.16	+1.53	44.18 \pm 0.55	+3.98
Only Diversity Distance	57.75 \pm 1.48	+3.49	93.98 \pm 0.24	+0.70	78.96 \pm 0.31	+0.67	43.84 \pm 0.19	+3.64
UDS (Full)	63.34\pm0.36	+9.08	95.19\pm0.22	+1.91	79.91\pm0.23	+2.22	46.28\pm0.35	+6.08

ing GREATS by +5.15% when using Qwen-2.5-7B. Similar gains appear on ScienceQA (95.19% vs. 94.17%), GSM8K (79.91% vs. 78.61%), and HumanEval (46.28% vs. 45.04%). The improvements hold across both Llama-3.1-8B and Qwen-2.5-7B, showing strong generalization. Overall, UDS surpasses simple heuristics (MaxLoss, MaxGrad) and advanced baselines (RHO-Loss, GREATS), achieving SOTA performance in the online batch selection setting.

UDS is more efficient than training on the full dataset. Beyond accuracy, UDS maintains competitive efficiency relative to training on the full dataset. On Qwen-2.5-7B, it achieves 3.41 samples/s on MMLU and 6.81 on HumanEval, both higher than those of full-dataset training (2.27 and 6.24). On Llama-3.1-8B, it also sustains higher throughput while yielding better accuracy. MaxLoss also trains quickly but provides only marginal accuracy gains, whereas MaxGrad slows training dramatically with no significant benefit. GREATS, though accurate, consistently runs slower than UDS. Thus, UDS achieves the best trade-off, combining high accuracy with efficiency.

4.3 ABLATION STUDIES

Both components of UDS contribute to performance. We conduct ablation studies on the two components of UDS, as summarized in Table 4. Using only the *Nuclear Norm* consistently outperforms random selection, underscoring the importance of capturing intra-sample utility and diversity. Using only the *Diversity Distance* also improves performance over the baseline, as discouraging redundancy among selected samples enhances overall utility. Combined, the two components complement each other to achieve the best results across all benchmarks, highlighting the necessity of jointly modeling sample utility, intra-sample diversity, and inter-sample diversity.

4.4 COMPARISON ACROSS DIFFERENT DATA SCALES

To assess the effectiveness of UDS under varying batch selection fractions, we conduct experiments as shown in Figure 4, where the horizontal axis denotes the number of selected samples K per batch and the vertical axis reports average accuracy.

While most methods improve with K , UDS’s performance peaks at $K = 4$, achieving the highest accuracy before gradually declines as additional, less informative samples are added. When $K = B = 8$, all methods reduce to full-dataset fine-tuning. UDS consistently outperforms baselines, showing its ability to prioritize informative and diverse samples. At its peak, UDS even surpasses full-dataset fine-tuning, demonstrating that a small, well-curated subset can deliver both efficiency and accuracy. These results confirm that UDS effectively balances exploitation and exploration, yielding robust improvements under different selection budgets.

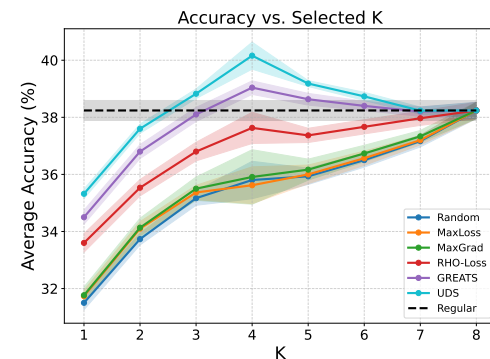


Figure 4: **Performance across different data scales using Llama-3.1-8B on MMLU.** We report accuracy when fine-tuning with varying proportions of training data. While all methods improve with more data, UDS consistently achieves the best accuracy and surpasses full-dataset fine-tuning.

5 CONCLUSION

In this work, we systematically analyze the limitations of current online batch selection methods for supervised fine-tuning of LLMs and establish three fundamental desiderata for optimal selection strategy design. To fulfill these requirements, we propose UDS, a novel framework that synergistically combines two complementary components: (i) Nuclear Norm scoring to capture both optimization utility and intra-sample diversity, and (ii) Diversity Distance measurement to ensure inter-sample diversity through efficient historical comparison. Extensive experiments across multiple domains illustrate UDS’s superior performance over existing methods while maintaining computational efficiency. Our approach provides a competitive and practical solution for effective online batch selection and holds the potential of scaling to more efficient LLM training scenarios.

REFERENCES

Josh Achiam, Steven Adler, Sandhini Agarwal, Lama Ahmad, Ilge Akkaya, Florencia Leoni Aleman, Diogo Almeida, Janko Altenschmidt, Sam Altman, Shyamal Anadkat, et al. Gpt-4 technical report. *arXiv preprint arXiv:2303.08774*, 2023.

Nir Ailon and Bernard Chazelle. Approximate nearest neighbors and the fast johnson-lindenstrauss transform. In *Proceedings of the thirty-eighth annual ACM symposium on Theory of computing*, pp. 557–563, 2006.

Nir Ailon and Bernard Chazelle. The fast johnson–lindenstrauss transform and approximate nearest neighbors. *SIAM Journal on computing*, 39(1):302–322, 2009.

Alon Albalak, Yanai Elazar, Sang Michael Xie, Shayne Longpre, Nathan Lambert, Xinyi Wang, Niklas Muennighoff, Bairu Hou, Liangming Pan, Haewon Jeong, et al. A survey on data selection for language models. *arXiv preprint arXiv:2402.16827*, 2024.

Jinze Bai, Shuai Bai, Yunfei Chu, Zeyu Cui, Kai Dang, Xiaodong Deng, Yang Fan, Wenbin Ge, Yu Han, Fei Huang, et al. Qwen technical report. *arXiv preprint arXiv:2309.16609*, 2023.

Tom Brown, Benjamin Mann, Nick Ryder, Melanie Subbiah, Jared D Kaplan, Prafulla Dhariwal, Arvind Neelakantan, Pranav Shyam, Girish Sastry, Amanda Askell, et al. Language models are few-shot learners. *Advances in neural information processing systems*, 33:1877–1901, 2020.

Sahil Chaudhary. Code alpaca: An instruction-following llama model for code generation. <https://github.com/sahil280114/codealpaca>, 2023.

Lichang Chen, Shiyang Li, Jun Yan, Hai Wang, Kalpa Gunaratna, Vikas Yadav, Zheng Tang, Vijay Srinivasan, Tianyi Zhou, Heng Huang, et al. Alpagasus: Training a better alpaca with fewer data. *arXiv preprint arXiv:2307.08701*, 2023.

Mark Chen, Jerry Tworek, Heewoo Jun, Qiming Yuan, Henrique Ponde de Oliveira Pinto, Jared Kaplan, Harri Edwards, Yuri Burda, Nicholas Joseph, Greg Brockman, Alex Ray, Raul Puri, Gretchen Krueger, Michael Petrov, Heidy Khlaaf, Girish Sastry, Pamela Mishkin, Brooke Chan, Scott Gray, Nick Ryder, Mikhail Pavlov, Alethea Power, Lukasz Kaiser, Mohammad Bavarian, Clemens Winter, Philippe Tillet, Felipe Petroski Such, Dave Cummings, Matthias Plappert, Fotios Chantzis, Elizabeth Barnes, Ariel Herbert-Voss, William Hebbgen Guss, Alex Nichol, Alex Paino, Nikolas Tezak, Jie Tang, Igor Babuschkin, Suchir Balaji, Shantanu Jain, William Saunders, Christopher Hesse, Andrew N. Carr, Jan Leike, Josh Achiam, Vedant Misra, Evan Morikawa, Alec Radford, Matthew Knight, Miles Brundage, Mira Murati, Katie Mayer, Peter Welinder, Bob McGrew, Dario Amodei, Sam McCandlish, Ilya Sutskever, and Wojciech Zaremba. Evaluating large language models trained on code, 2021.

Karl Cobbe, Vineet Kosaraju, Mohammad Bavarian, Mark Chen, Heewoo Jun, Lukasz Kaiser, Matthias Plappert, Jerry Tworek, Jacob Hilton, Reiichiro Nakano, Christopher Hesse, and John Schulman. Training verifiers to solve math word problems. *arXiv preprint arXiv:2110.14168*, 2021.

Zhijie Deng, Peng Cui, and Jun Zhu. Towards accelerated model training via bayesian data selection. *Advances in Neural Information Processing Systems*, 36:8513–8527, 2023.

Jiahui Geng, Fengyu Cai, Yuxia Wang, Heinz Koepll, Preslav Nakov, and Iryna Gurevych. A survey of confidence estimation and calibration in large language models. *arXiv preprint arXiv:2311.08298*, 2023.

Aaron Grattafiori, Abhimanyu Dubey, Abhinav Jauhri, Abhinav Pandey, Abhishek Kadian, Ahmad Al-Dahle, Aiesha Letman, Akhil Mathur, Alan Schelten, Alex Vaughan, et al. The llama 3 herd of models. *arXiv preprint arXiv:2407.21783*, 2024.

Dan Hendrycks, Collin Burns, Steven Basart, Andy Zou, Mantas Mazeika, Dawn Song, and Jacob Steinhardt. Measuring massive multitask language understanding. *Proceedings of the International Conference on Learning Representations (ICLR)*, 2021.

Roger A Horn and Charles R Johnson. *Matrix analysis*. Cambridge university press, 2012.

Yuheng Huang, Jiayang Song, Zhijie Wang, Shengming Zhao, Huaming Chen, Felix Juefei-Xu, and Lei Ma. Look before you leap: An exploratory study of uncertainty measurement for large language models. *arXiv preprint arXiv:2307.10236*, 2023.

Angela H Jiang, Daniel L-K Wong, Giulio Zhou, David G Andersen, Jeffrey Dean, Gregory R Ganger, Gauri Joshi, Michael Kaminsky, Michael Kozuch, Zachary C Lipton, et al. Accelerating deep learning by focusing on the biggest losers. *arXiv preprint arXiv:1910.00762*, 2019.

Ruhui Jin, Tamara G Kolda, and Rachel Ward. Faster johnson–lindenstrauss transforms via kronecker products. *Information and Inference: A Journal of the IMA*, 10(4):1533–1562, 2021.

William B Johnson, Joram Lindenstrauss, et al. Extensions of lipschitz mappings into a hilbert space. *Contemporary mathematics*, 26(189-206):1, 1984.

Jean Kaddour, Oscar Key, Piotr Nawrot, Pasquale Minervini, and Matt J Kusner. No train no gain: Revisiting efficient training algorithms for transformer-based language models. *Advances in Neural Information Processing Systems*, 36:25793–25818, 2023.

Angelos Katharopoulos and François Fleuret. Not all samples are created equal: Deep learning with importance sampling. In *International conference on machine learning*, pp. 2525–2534. PMLR, 2018.

Diederik P Kingma and Jimmy Ba. Adam: A method for stochastic optimization. *arXiv preprint arXiv:1412.6980*, 2014.

Katherine Lee, Daphne Ippolito, Andrew Nystrom, Chiyuan Zhang, Douglas Eck, Chris Callison-Burch, and Nicholas Carlini. Deduplicating training data makes language models better. *arXiv preprint arXiv:2107.06499*, 2021.

Dengchun Li, Yingzi Ma, Naizheng Wang, Zhengmao Ye, Zhiyuan Cheng, Yinghao Tang, Yan Zhang, Lei Duan, Jie Zuo, Cal Yang, et al. Mixlora: Enhancing large language models fine-tuning with lora-based mixture of experts. *arXiv preprint arXiv:2404.15159*, 2024.

Aixin Liu, Bei Feng, Bing Xue, Bingxuan Wang, Bochao Wu, Chengda Lu, Chenggang Zhao, Chengqi Deng, Chenyu Zhang, Chong Ruan, et al. Deepseek-v3 technical report. *arXiv preprint arXiv:2412.19437*, 2024.

Antonio Loquercio, Mattia Segu, and Davide Scaramuzza. A general framework for uncertainty estimation in deep learning. *IEEE Robotics and Automation Letters*, 5(2):3153–3160, 2020.

Ilya Loshchilov and Frank Hutter. Online batch selection for faster training of neural networks. *arXiv preprint arXiv:1511.06343*, 2015.

Pan Lu, Swaroop Mishra, Tony Xia, Liang Qiu, Kai-Wei Chang, Song-Chun Zhu, Oyvind Tafjord, Peter Clark, and Ashwin Kalyan. Learn to explain: Multimodal reasoning via thought chains for science question answering. In *The 36th Conference on Neural Information Processing Systems (NeurIPS)*, 2022.

Sören Mindermann, Jan M Brauner, Muhammed T Razzak, Mrinank Sharma, Andreas Kirsch, Winnie Xu, Benedikt Höltgen, Aidan N Gomez, Adrien Morisot, Sebastian Farquhar, et al. Prioritized training on points that are learnable, worth learning, and not yet learnt. In *International Conference on Machine Learning*, pp. 15630–15649. PMLR, 2022.

Ru Peng, Heming Zou, Haobo Wang, Yawen Zeng, Zenan Huang, and Junbo Zhao. Energy-based automated model evaluation. *arXiv preprint arXiv:2401.12689*, 2024.

Xin Qiu and Risto Miikkulainen. Semantic density: Uncertainty quantification for large language models through confidence measurement in semantic space. *Advances in neural information processing systems*, 37:134507–134533, 2024.

Pengzhen Ren, Yun Xiao, Xiaojun Chang, Po-Yao Huang, Zhihui Li, Brij B Gupta, Xiaojiang Chen, and Xin Wang. A survey of deep active learning. *ACM computing surveys (CSUR)*, 54(9):1–40, 2021.

Ola Shorinwa, Zhiting Mei, Justin Lidard, Allen Z Ren, and Anirudha Majumdar. A survey on uncertainty quantification of large language models: Taxonomy, open research challenges, and future directions. *ACM Computing Surveys*, 2025.

Kushal Tirumala, Daniel Simig, Armen Aghajanyan, and Ari Morcos. D4: Improving llm pretraining via document de-duplication and diversification. *Advances in Neural Information Processing Systems*, 36:53983–53995, 2023.

Hugo Touvron, Thibaut Lavril, Gautier Izacard, Xavier Martinet, Marie-Anne Lachaux, Timothée Lacroix, Baptiste Rozière, Naman Goyal, Eric Hambro, Faisal Azhar, et al. Llama: Open and efficient foundation language models. *arXiv preprint arXiv:2302.13971*, 2023.

Joel A Tropp. Improved analysis of the subsampled randomized hadamard transform. *Advances in Adaptive Data Analysis*, 3(01n02):115–126, 2011.

Jiachen Tianhao Wang, Tong Wu, Dawn Song, Prateek Mittal, and Ruoxi Jia. Greats: Online selection of high-quality data for llm training in every iteration. *Advances in Neural Information Processing Systems*, 37:131197–131223, 2024.

Yizhong Wang, Yeganeh Kordi, Swaroop Mishra, Alisa Liu, Noah A Smith, Daniel Khashabi, and Hannaneh Hajishirzi. Self-instruct: Aligning language models with self-generated instructions. *arXiv preprint arXiv:2212.10560*, 2022.

Alexander Wettig, Aatmik Gupta, Saumya Malik, and Danqi Chen. Qurating: Selecting high-quality data for training language models. *arXiv preprint arXiv:2402.09739*, 2024.

Mengzhou Xia, Sadhika Malladi, Suchin Gururangan, Sanjeev Arora, and Danqi Chen. Less: Selecting influential data for targeted instruction tuning. *arXiv preprint arXiv:2402.04333*, 2024.

Sang Michael Xie, Shibani Santurkar, Tengyu Ma, and Percy S Liang. Data selection for language models via importance resampling. *Advances in Neural Information Processing Systems*, 36: 34201–34227, 2023.

Benfeng Xu, Licheng Zhang, Zhendong Mao, Quan Wang, Hongtao Xie, and Yongdong Zhang. Curriculum learning for natural language understanding. In *Proceedings of the 58th annual meeting of the association for computational linguistics*, pp. 6095–6104, 2020.

An Yang, Baosong Yang, Beichen Zhang, Binyuan Hui, Bo Zheng, Bowen Yu, Chengyuan Li, Dayiheng Liu, Fei Huang, Haoran Wei, et al. Qwen2. 5 technical report. *arXiv preprint arXiv:2412.15115*, 2024.

Chunting Zhou, Pengfei Liu, Puxin Xu, Srinivasan Iyer, Jiao Sun, Yuning Mao, Xuezhe Ma, Avia Efrat, Ping Yu, Lili Yu, et al. Lima: Less is more for alignment. *Advances in Neural Information Processing Systems*, 36:55006–55021, 2023.

Heming Zou, Yunliang Zang, Wutong Xu, Yao Zhu, and Xiangyang Ji. Flylora: Boosting task decoupling and parameter efficiency via implicit rank-wise mixture-of-experts. *arXiv preprint arXiv:2510.08396*, 2025.

A RELATED WORK

Online Batch Selection for Large Language Models. Several studies have investigated online batch selection prior to the era of LLMs. Works like (Jiang et al., 2019; Katharopoulos & Fleuret, 2018; Loshchilov & Hutter, 2015) propose heuristic methods that select “important” samples (e.g., via high training loss, or large gradient norm). These methods are straightforward and often effective for smaller models or simpler tasks, but more recent studies (Wang et al., 2024) show that these heuristics may not scale well for LLMs. Another paradigm uses a reference model to help evaluate sample importance. For instance, (Deng et al., 2023; Minderhout et al., 2022) use a pre-trained or separately trained reference model, and select samples based on how “different” they are relative to that model. These methods tend to require extra computation (e.g. extra forward passes) and sometimes held-out data to train the reference model, which can make them costly or impractical in large-scale LLM training. (Kaddour et al., 2023) points out that these overheads can outweigh benefits in many settings. GREATS (Wang et al., 2024) is a more recent SOTA method. It selects data batches online by considering loss reduction on a validation set, and uses a “ghost inner-product” approximation (via a Taylor-expansion-based greedy algorithm) to accelerate selection. However, the need for a validation set may be unavailable or non-representative in practical deployment (Wang et al., 2024).

Offline Data Selection for Large Language Models. Most existing approaches to data selection are performed in an offline manner, where samples are filtered prior to training (Albalak et al., 2024; Xia et al., 2024; Zhou et al., 2023; Chen et al., 2023; Xie et al., 2023; Wettig et al., 2024). This is primarily due to efficiency concerns, since curating the entire dataset at every iteration is prohibitively expensive. Early approaches extend uncertainty estimation and active learning heuristics, such as filtering by entropy or difficulty, but these remain limited in capturing truly informative samples (Xu et al., 2020). A more impactful direction is large-scale pruning and deduplication: (Lee et al., 2021; Tirumala et al., 2023) show that removing near-duplicate or low-quality data improves efficiency and prevents overfitting. In instruction tuning, several works highlight that “quality outweighs quantity”, with methods like LIMA (Zhou et al., 2023), LESS (Xia et al., 2024), and Self-Instruct (Wang et al., 2022) filtering diverse, representative subsets while discarding noisy prompts. While effective to some extent, this perspective assumes that the value of each example is fixed throughout the learning process. In reality, learning is highly dynamic. Data that appear highly informative at the beginning of training may later become redundant (Wang et al., 2024). This limitation motivates serving online batch selection as a complement for dynamically assessing sample value during the training process.

B ADDITIONAL RESULTS

B.1 PARAMETER ANALYSIS

Impact of memory buffer size and low projected dimension. We evaluate the influence of the projected dimensions d_1 , d_2 , and the memory buffer size M on both model performance and resource usage. As shown in Figures 5 and 6, increasing the projected dimensions and memory buffer consistently improves accuracy, which gradually saturates once d_1 , d_2 , and M become sufficiently large. The trends of d_1 and d_2 are consistent with the Johnson-Lindenstrauss lemma (Johnson et al., 1984; Ailon & Chazelle, 2006; Jin et al., 2021; Ailon & Chazelle, 2009; Tropp, 2011), while a sufficiently large M leads to performance saturation, indicating that the stored representations are adequate to capture global sample diversity. The corresponding increases in memory usage and computation time are minor, and arise only when computing inter-sample diversity.

In Figure 5, increasing d_1 , d_2 , and M has no significant impact on extra memory usage. The base overhead of around 1.17GB comes from the projection matrices Γ_1 and Γ_2 , which is small compared to the overall training memory footprint of about 22GB. In Figure 6, the additional time per batch is also negligible relative to the total training cost of 2.3s per batch.

Overall, the extra resource cost is minimal compared to the performance gains. In practice, parameter selection only needs to ensure that d_1 , d_2 , and M are sufficiently large for stable performance.

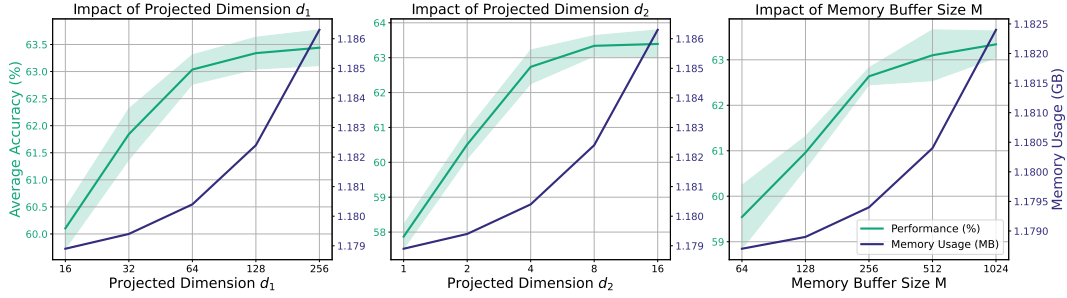


Figure 5: **Impact of low projected dimensions d_1 and d_2 , and memory buffer size M on model performance and additional memory usage for Qwen-2.5 on MMLU.** The green curves show average accuracy (%), and the blue curves show extra peak memory consumption (GB). Performance improves with increasing projected dimensions and memory buffer size, while additional memory usage increases only slightly.

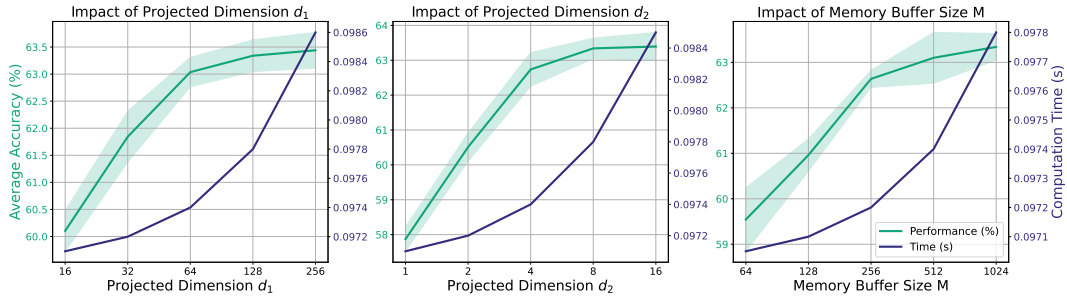


Figure 6: **Impact of low projected dimensions d_1 and d_2 , and memory buffer size M on model performance and additional computation time for Qwen-2.5 on MMLU.** The green curves show average accuracy (%), and the blue curves show additional computation time per batch (s). Performance improves with increasing projected dimensions and memory buffer size, while the additional computation time remains negligible.

Impact of trade-off factor α . Figure 7 presents the sensitivity analysis of α on Qwen-2.5-7B across four datasets. The results consistently exhibit an inverted U-shaped trend: performance improves as α increases, peaks at an optimal value, and then declines as α continues to grow. This pattern highlights the importance of maintaining a proper balance. The optimal α values corresponding to the selected data fractions in Table 5 are summarized in Table 6.

Table 5: **Data selection fractions across benchmark datasets.** Percentages of samples selected from MMLU, ScienceQA, GSM8K, and CodeAlpaca, evaluated with Llama-3.1-8B and Qwen-2.5-7B as backbone models.

Model	MMLU	ScienceQA	GSM8K	CodeAlpaca
Llama-3.1-8B	50%	50%	50%	50%
Qwen-2.5-7B	12.5%	50%	25%	50%

C THEORETICAL ANALYSIS

C.1 RELATIONSHIP BETWEEN FROBENIUS NORM AND NUCLEAR NORM

Lemma 3.1 establishes a fundamental relationship between two widely used matrix norms: the Frobenius norm $\|\cdot\|_F$ and the nuclear norm $\|\cdot\|_*$. Recall that if $\mathbf{L}(x_t^i; \theta_t) \in \mathbb{R}^{N \times V}$ has singular

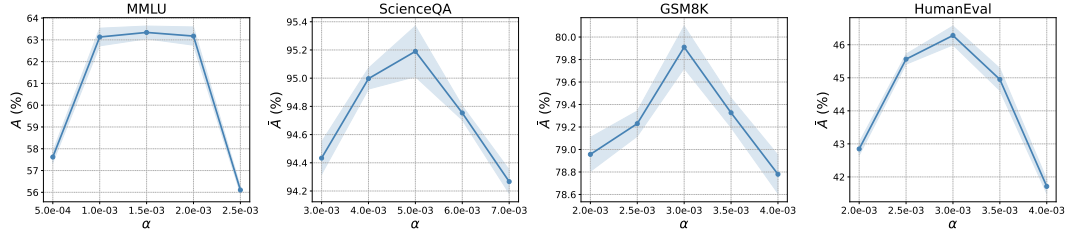


Figure 7: **Sensitivity analysis of the trade-off factor α on Qwen-2.5-7B.** Results are reported across four benchmarks—MMLU, ScienceQA, GSM8K, and HumanEval—using the data selection fractions specified in Table 5.

Table 6: **Optimal trade-off factor α across datasets and backbones.** Optimal α values for MMLU, ScienceQA, GSM8K, and CodeAlpaca using Llama-3.1-8B and Qwen-2.5-7B, with data selection fractions given in Table 5.

Model	MMLU	ScienceQA	GSM8K	CodeAlpaca
Llama-3.1-8B	4.5×10^{-3}	7×10^{-3}	1×10^{-3}	5×10^{-3}
Qwen-2.5-7B	1.5×10^{-3}	5×10^{-3}	3×10^{-3}	3×10^{-3}

values $\{\sigma_j\}_{j=1}^r$ with rank $r \leq \min(N, V)$, then

$$\|\mathbf{L}(\mathbf{x}_t^i; \boldsymbol{\theta}_t)\|_F = \left(\sum_{j=1}^r \sigma_j^2 \right)^{1/2}, \quad \|\mathbf{L}(\mathbf{x}_t^i; \boldsymbol{\theta}_t)\|_* = \sum_{j=1}^r \sigma_j. \quad (13)$$

The two-sided inequality in Lemma 3.1 is proved as follows.

(1) *Lower bound.* Since the Euclidean norm of a set of nonnegative numbers is always no larger than their sum, we have

$$\|\mathbf{L}(\mathbf{x}_t^i; \boldsymbol{\theta}_t)\|_F = \left(\sum_{j=1}^r \sigma_j^2 \right)^{1/2} \leq \sum_{j=1}^r \sigma_j = \|\mathbf{L}(\mathbf{x}_t^i; \boldsymbol{\theta}_t)\|_*. \quad (14)$$

Equality holds iff at most one singular value is nonzero, i.e., $\mathbf{L}(\mathbf{x}_t^i; \boldsymbol{\theta}_t)$ is rank-1 (in which case the Euclidean norm and the sum of singular values coincide).

(2) *Upper bound.* Applying the Cauchy–Schwarz inequality to the vectors $(1, \dots, 1) \in \mathbb{R}^r$ and $(\sigma_1, \dots, \sigma_r) \in \mathbb{R}^r$ yields

$$\|\mathbf{L}(\mathbf{x}_t^i; \boldsymbol{\theta}_t)\|_* = \sum_{j=1}^r \sigma_j \leq \left(\sum_{j=1}^r 1^2 \right)^{1/2} \left(\sum_{j=1}^r \sigma_j^2 \right)^{1/2} = \sqrt{r} \|\mathbf{L}(\mathbf{x}_t^i; \boldsymbol{\theta}_t)\|_F. \quad (15)$$

Since $r \leq \min(N, V)$ we obtain the stated upper bound

$$\|\mathbf{L}(\mathbf{x}_t^i; \boldsymbol{\theta}_t)\|_* \leq \sqrt{\min(N, V)} \|\mathbf{L}(\mathbf{x}_t^i; \boldsymbol{\theta}_t)\|_F. \quad (16)$$

Equality in the Cauchy–Schwarz step holds iff the singular-value vector is proportional to the all-ones vector, i.e. all nonzero singular values are equal. Thus the rightmost equality is achieved when $r = \min(N, V)$ (full possible rank) and the r singular values are equal.

Implications. This lemma highlights that the nuclear norm and Frobenius norm, though correlated, capture different structural aspects of $\mathbf{L}(\mathbf{x}_t^i; \boldsymbol{\theta}_t)$. The Frobenius norm measures the overall magnitude of logits, while the nuclear norm is also sensitive to their rank structure. A large nuclear norm relative to the Frobenius norm implies more “spread-out” singular values and thus higher intra-sample diversity.

C.2 OPTIMIZATION ANALYSIS USING ADAM

When using the Adam (Kingma & Ba, 2014) as optimizer, the parameter update at step t is

$$\boldsymbol{\theta}_{t+1} - \boldsymbol{\theta}_t = -\eta_t \cdot \frac{\hat{\mathbf{m}}_t}{\sqrt{\hat{\mathbf{v}}_t} + \epsilon_{\text{adam}}}, \quad (17)$$

where $\hat{\mathbf{m}}_t$ and $\hat{\mathbf{v}}_t$ are the bias-corrected first and second moment estimates of the stochastic gradients, respectively:

$$\hat{\mathbf{m}}_t = \frac{\mathbf{m}_t}{1 - \beta_1^t}, \quad \hat{\mathbf{v}}_t = \frac{\mathbf{v}_t}{1 - \beta_2^t}, \quad \mathbf{m}_t = \beta_1 \mathbf{m}_{t-1} + (1 - \beta_1) \cdot \mathbf{g}_t, \quad \mathbf{v}_t = \beta_2 \mathbf{v}_{t-1} + (1 - \beta_2) \cdot \mathbf{g}_t^2, \quad (18)$$

with $\mathbf{g}_t = \frac{1}{B} \sum_{i=1}^B \nabla_{\boldsymbol{\theta}} \ell(\mathbf{x}_t^i; \boldsymbol{\theta}_t)$.

After the parameter update $\boldsymbol{\theta}_t \rightarrow \boldsymbol{\theta}_{t+1}$, the logits matrix for datapoint \mathbf{x}_t^i can be expanded using a first-order Taylor expansion:

$$\mathbf{L}(\mathbf{x}_t^i; \boldsymbol{\theta}_{t+1}) \approx \mathbf{L}(\mathbf{x}_t^i; \boldsymbol{\theta}_t) + \nabla_{\boldsymbol{\theta}} \mathbf{L}(\mathbf{x}; \boldsymbol{\theta}_t) \cdot (\boldsymbol{\theta}_{t+1} - \boldsymbol{\theta}_t), \quad (19)$$

so that the induced change is

$$\delta \mathbf{L}(\mathbf{x}; \boldsymbol{\theta}_t) \approx -\eta_t \nabla_{\boldsymbol{\theta}} \mathbf{L}(\mathbf{x}; \boldsymbol{\theta}_t) \cdot \frac{\hat{\mathbf{m}}_t}{\sqrt{\hat{\mathbf{v}}_t} + \epsilon_{\text{adam}}}. \quad (20)$$

C.3 DISTANCE PRESERVATION UNDER LOW-DIMENSIONAL PROJECTION

We show that our two-sided projection construction can be algebraically reduced to a single sub-sampled randomized Fourier transform (SRFT) on \mathbb{R}^{NV} . Recall the standard property of the vec operator with Kronecker products: for conformable matrices $\mathbf{A}, \mathbf{B}, \mathbf{X}$, we have

$$\text{vec}(\mathbf{A} \mathbf{X} \mathbf{B}) = (\mathbf{B}^\top \otimes \mathbf{A}) \text{vec}(\mathbf{X}). \quad (21)$$

Applying this to $\boldsymbol{\Gamma}_2 \in \mathbb{R}^{d_2 \times N}$, $\boldsymbol{\Gamma}_1 \in \mathbb{R}^{d_1 \times V}$, and $\mathbf{L}(\mathbf{x}_t^i; \boldsymbol{\theta}_t) \in \mathbb{R}^{N \times V}$, we obtain

$$\mathbf{z}_t^i = \text{vec}(\boldsymbol{\Gamma}_2 \mathbf{L}(\mathbf{x}_t^i; \boldsymbol{\theta}_t) \boldsymbol{\Gamma}_1^\top) = (\boldsymbol{\Gamma}_1 \otimes \boldsymbol{\Gamma}_2) \text{vec}(\mathbf{L}(\mathbf{x}_t^i; \boldsymbol{\theta}_t)) = \boldsymbol{\Gamma} \text{vec}(\mathbf{L}(\mathbf{x}_t^i; \boldsymbol{\theta}_t)), \quad (22)$$

where $\boldsymbol{\Gamma} = \boldsymbol{\Gamma}_1 \otimes \boldsymbol{\Gamma}_2 \in \mathbb{R}^{d_1 d_2 \times NV}$. Using the Kronecker identity $(\mathbf{A} \otimes \mathbf{B})(\mathbf{C} \otimes \mathbf{D}) = (\mathbf{A}\mathbf{C}) \otimes (\mathbf{B}\mathbf{D})$, we can rewrite

$$\boldsymbol{\Gamma} = \left(\sqrt{\frac{V}{d_1}} \mathbf{S}_1 \mathbf{F}_1 \mathbf{D}_1 \right) \otimes \left(\sqrt{\frac{N}{d_2}} \mathbf{S}_2 \mathbf{F}_2 \mathbf{D}_2 \right) \quad (23)$$

$$= \sqrt{\frac{NV}{d_1 d_2}} (\mathbf{S}_1 \otimes \mathbf{S}_2) (\mathbf{F}_1 \otimes \mathbf{F}_2) (\mathbf{D}_1 \otimes \mathbf{D}_2), \quad (24)$$

where $\mathbf{S} = \mathbf{S}_1 \otimes \mathbf{S}_2$, $\mathbf{F} = \mathbf{F}_1 \otimes \mathbf{F}_2$, and $\mathbf{D} = \mathbf{D}_1 \otimes \mathbf{D}_2$. Since each \mathbf{F}_i is orthonormal and \mathbf{D}_i has independent Rademacher entries, \mathbf{F} is orthonormal and \mathbf{D} remains a diagonal matrix with independent Rademacher entries. Hence, $\boldsymbol{\Gamma} = \sqrt{\frac{NV}{d_1 d_2}} \mathbf{S} \mathbf{F} \mathbf{D}$ is exactly an SRFT.

Remark: This Kronecker structure preserves the SRFT type. In contrast, if $\boldsymbol{\Gamma}_1, \boldsymbol{\Gamma}_2$ are i.i.d. Gaussian (as in classical JL), then $\boldsymbol{\Gamma}_1 \otimes \boldsymbol{\Gamma}_2$ no longer has i.i.d. Gaussian entries due to induced correlations.

Johnson-Lindenstrauss Guarantee. Let $\mathbf{u}_1, \dots, \mathbf{u}_n \in \mathbb{R}^{NV}$ denote n vectors of interest. Consider all pairwise differences $\mathbf{u}_i - \mathbf{u}_j$, $1 \leq i < j \leq n$; there are at most $n(n-1)/2$ such vectors. By standard results on Fast JL transforms (SRFT/FJLT) (Ailon & Chazelle, 2006; Jin et al., 2021; Ailon & Chazelle, 2009; Tropp, 2011), for any $0 < \epsilon < 1$ and a fixed set of n vectors in \mathbb{R}^{NV} , a random SRFT $\boldsymbol{\Gamma} \in \mathbb{R}^{d_1 d_2 \times NV}$ preserves the ℓ_2 norms up to $(1 \pm \epsilon)$ with high probability provided

$$d_1 d_2 \gtrsim C \epsilon^{-2} \log(NV) \text{polylog}(n), \quad (25)$$

where C is an absolute constant and the polylog factor depends on the SRFT construction. This gives that, with high probability, for all i, j :

$$(1 - \epsilon) \|\mathbf{u}_i - \mathbf{u}_j\|_2^2 \leq \|\boldsymbol{\Gamma}(\mathbf{u}_i - \mathbf{u}_j)\|_2^2 \leq (1 + \epsilon) \|\mathbf{u}_i - \mathbf{u}_j\|_2^2, \quad (26)$$

which is exactly the claimed Johnson-Lindenstrauss distance preservation.

D DETAILED EXPERIMENTAL SETTING

D.1 DATASETS

We conduct our experiments on the following datasets, with important information listed in Table 7. Brief introduction for each dataset are provided in the following:

- **MMLU** [Hendrycks et al. \(2021\)](#) is a benchmark designed to assess general knowledge understanding, consisting of multiple-choice questions from various branches of knowledge. It covers 57 tasks including elementary mathematics, US history, computer science, law, and more.
- **ScienceQA** [Lu et al. \(2022\)](#) is a multimodal science question answering dataset collected from elementary and high school science curricula, including multiple-choice problems that align with California Common Core Content Standards. The questions in dataset are sourced from open resources managed by IXL Learning, an online learning platform curated by experts in the field of K-12 education. We extract textual parts within it following [Li et al. \(2024\)](#).
- **GSM8K** [Cobbe et al. \(2021\)](#) is a dataset of 8.5K high quality linguistically diverse grade school math word problems, each requiring multi-step arithmetic reasoning. Answers are provided in a step-by-step explanation format.
- **CodeAlpaca-20k** [Chaudhary \(2023\)](#) is an instruction-following dataset consisting of 20k examples generated to align code-related prompts with helpful outputs. It is synthetically constructed to enhance code instruction tuning.
- **HumanEval** [Chen et al. \(2021\)](#) is a code generation benchmark including 164 Python programming problems. The dataset was handwritten to ensure not to be included in the training set of code generation models.

Table 7: **Details of MMLU, ScienceQA, GSM8K, CodeAlpaca and HumanEval Datasets.** We list the number of training and testing samples and task types for the following datasets used in our experiments.

Dataset	Training Samples	Testing Samples	Task Types
MMLU Hendrycks et al. (2021)	99842	14042	Multiple Choice
ScienceQA Lu et al. (2022)	12726	4241	Multiple Choice
GSM8K Cobbe et al. (2021)	7473	1319	Math Problems
CodeAlpaca-20k Chaudhary (2023)	20022	—	Code Instruction
HumanEval Chen et al. (2021)	—	164	Code Generation

D.2 TRAINING CONFIGURATION

In this section, we detail the experiment configuration with hyper parameters. General configurations across all backbones and datasets are listed in Table 8. Dataset-specific and model-specific setting are listed in Table 9. For all baseline approaches, we adopt the same configurations described above. For GREATS, we set the validation set size to 5. For RHO-Loss, we use Llama-2-13B as the reference model for Llama-3.1-8B, and Qwen-2.5-14B as the reference model for Qwen-2.5-7B. Ideally, Llama-3.1-70B would serve as a better reference model for Llama-3.1-8B, but its computational cost makes it impractical in our setting. Fortunately, we find that Llama-2-13B provides sufficiently strong guidance, and thus we adopt it as a surrogate reference model.

E LIMITATIONS AND FUTURE WORK

Limitations. One potential limitation of our framework lies in the computation of the nuclear norm. While it can be obtained directly from the singular values of the logits matrix without incurring additional expensive backpropagation, the SVD of large matrices may still introduce non-negligible overhead in practice, particularly for long sequences with large vocabulary sizes. We also explored approximate methods such as randomized SVD to accelerate the computation, but observed that the loss in precision often degrades the overall performance.

Table 8: **General Training Hyperparameters with LoRA.** Shared configuration across all experiments, including rank settings, optimizer details, and architectural choices.

Parameter	Value
Rank (r)	8
Scaling factor (α)	16
Target modules	{q, k, v, o, gate, down, up}-proj
Optimizer	AdamW
Warmup ratio	0.01
Gradient accumulated batch	128
Dropout rate	0.00

Table 9: **Dataset-Specific and Model-Specific Training Configurations during training.** Task-optimized settings for Llama-3.1-8B and Qwen-2.5-7B across four benchmarks, showing variations in epoch counts, learning rates, and sequence lengths based on dataset characteristics and model requirements.

Model	Parameter	MMLU	ScienceQA	GSM8K	CodeAlpaca
Llama-3.1-8B	Epochs	1	20	1	2
	Learning rate	1.5×10^{-4}	3×10^{-4}	3×10^{-4}	3×10^{-4}
	Max sequence length	512	256	512	512
	micro batch size	8	8	8	8
Qwen-2.5-7B	Epochs	1	20	1	2
	Learning rate	1.5×10^{-4}	3×10^{-4}	3×10^{-4}	3×10^{-4}
	Max sequence length	512	256	512	512
	micro batch size	8	8	8	8

Future Work. An important future direction is to explore more efficient and accurate estimators of the nuclear norm. Potential avenues include exploiting structured low-rank approximations, leveraging iterative or block-wise SVD techniques, or designing surrogate scoring functions that preserve the optimization and diversity signals of the nuclear norm while being cheaper to compute. Such improvements would further enhance the scalability of our framework to larger models and longer input sequences. Furthermore, techniques in uncertainty estimation or active learning may be other promising directions for online batch selection (Ren et al., 2021; Loquercio et al., 2020; Peng et al., 2024).

F LLM USAGE DECLARATION

In preparing this manuscript, we used a large language model solely as a language assistance tool. Specifically, the LLM was employed to polish the phrasing of certain paragraphs and to improve clarity and readability of the text. All technical ideas, derivations, experiments, and analyses were conceived, implemented, and validated entirely by the authors. The LLM was not used for generating research ideas, designing experiments, or producing novel scientific content. The authors take full responsibility for all contents of the paper.